Hindawi
Shock and Vibration
Volume 2021, Article ID 2847603, 14 pages
https://doi.org/10.1155/2021/2847603

Research Article

Lateral Seismic Fragility Assessment of Cable-Stayed Bridge with Diamond-Shaped Concrete Pylons

Chao Zhang,[1] **Jianbin Lu**,[1] **Zhengan Zhou**,[1] **Xueyuan Yan**,[1] **Li Xu**,[1] **and Jinjun Lin**[2]

[1]*College of Civil Engineering, Fuzhou University, Fuzhou 35002, China*
[2]*Fuzhou New Area Development Investment Group Co., Ltd., Fuzhou 35002, China*

Correspondence should be addressed to Xueyuan Yan; yxy820910@sina.com

Received 17 June 2021; Accepted 6 August 2021; Published 17 August 2021

Academic Editor: Kaiming Bi

Copyright © 2021 Chao Zhang et al. This is an open access article distributed under the Creative Commons Attribution License, which permits unrestricted use, distribution, and reproduction in any medium, provided the original work is properly cited.

The cable-stayed bridge with diamond-shaped pylons is one of the most popular bridges because of its obvious advantages such as aesthetical appearance and smaller foundation. However, the diamond-shaped pylons have both inward and outward inclinations, which may result in complicated seismic behavior when subjected to lateral earthquake excitations. To end this, the finite element model of a cable-stayed bridge with diamond concrete pylon is developed firstly. Four limit states and corresponding damage index are defined for each critical section. Finally, the lateral seismic fragility of the components and system of CSB was carried out. Based on the result of probabilistic estimation of lateral seismic responses, the order of the damage probability in all four damage states for each component of bridge is given. The fragility curves of bridge system on the lower bound and upper bound are studied. Moreover, the system fragility of the entire bridge is compared with that of each component.

1. Introduction

Cable-stayed bridge is featured by its appealing aesthetics, large spanning capacity, and excellent economic performance, which has been widely constructed around the world in the last several decades [1, 2]. The pylon is the most important component of the CSB system [3]. In general, the pylon should be designed to vertically resist large gravity load and also accommodate an amount of lateral loads associated with live loads, wind and earthquakes, and other possible loads [4]. The pylons in the regular cable-stayed bridges can be classified into five categories based upon their geometric configurations: H-, A-, inverted Y-, diamond-, and vase-shaped pylons (Figure 1). In the design of CSB, the width of the bridge pylon at the lower beam is determined by the width of the main girder. The inverted Y- and diamond-shaped pylons are splayed inward above the deck level which results in greater lateral stiffness than H-shape pylon [5]. Furthermore, the legs of the diamond-shaped pylon are carried down to the pile caps with the inward inclination, which produces a lower diamond. As a result, the diamond-shaped pylon has relatively smaller foundation and thus gives a potential saving for the construction cost compared with the inverted Y- and H-shaped pylons [6]. In general, diamond-shaped pylons are the most commonly adopted pylon types for the CSB [7].

Cable-stayed bridge always plays a significant role in the infrastructure networks, and hence it is important to ensure the structural safety and reliability under severe earthquakes [8, 9]. However, severe earthquake damages of cable-stayed bridges were found when subjected to a strong earthquake. During the 1999 Chi-Chi earthquake, the plastic hinges formed at the bottom of pylon, and the cracks were extended to the lowest cable for the Chi-Lu Cable-Stayed Bridge [10]. Moreover, the Yokohama-Bay Bridge which is a typical cable-stayed bridge with H-shaped pylons was damaged in the 2011 Great East Japan Earthquake. Its nuts and bolts on the link of deck-pylon connection were crushed due to the impact of the girder [11].

As typical cable-supported bridges, most CSBs are the floating system or semifloating system in longitudinal direction [12]. Owing to the flexibility and slenderness of the floating CSB system, a major portion of the earthquake energy can be dissipated during earthquakes [13], especially when energy

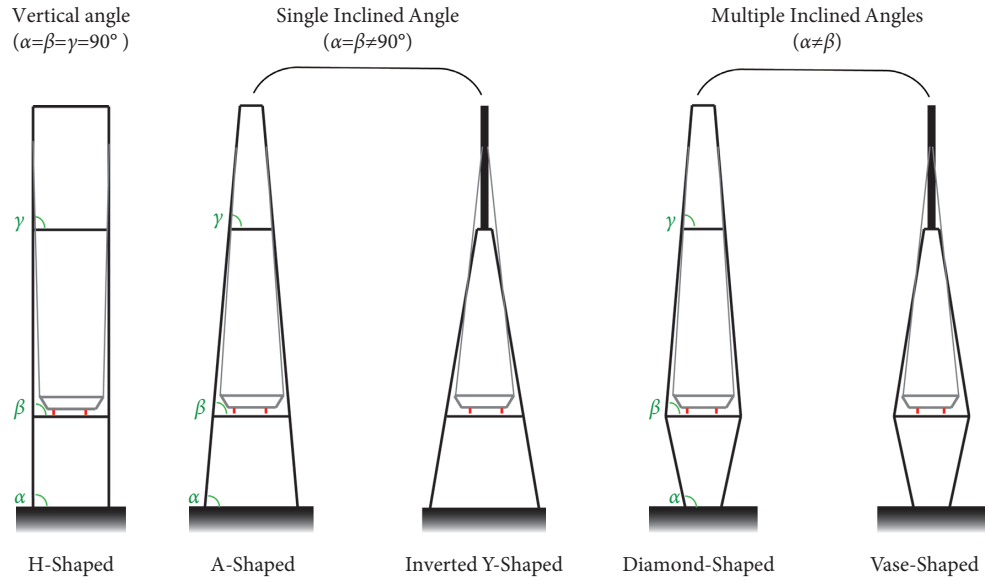

Figure 1: Different pylons in cable-stayed bridges.

dissipation devices are applied, such as viscous dampers [13]. Therefore, the longitudinal seismic performance of CSB is usually not bad [13–15]. However, the pylon-girder generally adopts fixed restraints in the transverse direction due to wind-resistant requirements. As a result, the huge lateral seismic inertial force of the girder will be directly transmitted to the pylons or piers. Therefore, pylons or piers usually need to withstand large seismic forces in the transverse direction. When encountering an earthquake that exceeds the fortification level, the pylons may be damage or yield. The damaged bridge tower during the 1999 Chi-Chi earthquake proves that the pylon of the CSB may make lateral damage. At present, the lateral seismic excitation case always is the critical case in the pylon design for the CSBs [16].

Several researchers have investigated the influence of earthquake ground motions on the transversal dynamic response of the cable-stayed bridge. For example, Xie and Sun [17] designed and assembled a 1/70-scaled bridge full-model of cable-stayed bridge, which was composed of the A-shaped pylons. Shaking table tests were conducted to study the seismic response and potential failure mode of pylons of the bridge full-model under transverse earthquake excitation. Test results show that the pylon exhibits an unexpected failure mode with the double plastic hinges. Han et al. [18] quantified the scouring effect on the seismic performance of a single pylon cable-stayed bridge under bidirectional earthquake excitations. Wang et al. [19] assessed the transverse seismic failure mechanism and ductile properties of typical inverted Y-shape RC pylons for long-span cable-stayed bridges using quasistatic model tests and numerical analyses. Guan et al. conducted a shaking table experiment based on a long-span cable-stayed bridge with typical inverted-Y-shaped towers. Wang et al. [20, 21] conducted a/20-scale full bridge model from a typical medium-span cable-stayed bridge to study the potential plastic region and possible failure mode of the concrete H-shaped pylon subjected to the transverse excitations.

Nevertheless, despite some researchers have investigated the seismic performance of A-, inverted Y-, and H-shaped pylons through dynamic tests and numerical simulations, limited attention has been paid to the seismic behavior of the widely used diamond-shaped pylons [22]. Previous studies show that pylon with inclined legs can be loaded with a combination of bending, torsion, shear, and axial force under earthquakes [6]. Especially diamond-shaped pylon, which has both inward and outward inclinations, may induce more complicated seismic behavior under earthquake excitations [23].

Previous studies on lateral seismic response of CSBs are mostly based on nonlinear time-history analysis or shaking table tests subjected to certain earthquakes. Due to the extreme discreteness of earthquakes, the seismic response law under certain or several earthquake excitations cannot be applied to guide the seismic design of the CSB. Seismic fragility analysis provides an important method for evaluating the seismic behaviors of bridge structures [24]. The assessment of the seismic performance of bridge can be assessed by fragility curves even in regions that lacked earthquake damage data [25]. Fragility analysis is an effective technique for the probabilistic assessment of seismic risk, which can help structural designers in the decision-making process to execute performance-based seismic design [26]. Li et al. [27] evaluated the seismic performance of a sea-crossing cable-stayed bridge based on the fragility function methodology. Zhong et al. [28] conducted a risk assessment for a long-span cable-stayed bridge subjected to multiple support excitations. Overall, the above studies mainly focus on the longitudinal seismic fragility performance of the CSB. Some scholars have carried out relevant research on the lateral seismic response of CSB with vertical or single inclined pylons. However, the biggest difference of diamond-shaped pylon comparing to vertical or single inclined pylons is that the pylon is designed with double inclined angles in the lateral direction. This design makes the lateral stiffness of the pylons change. At the same time, the lateral deformation law of the pylons changes

greatly. It is not clear whether the conclusion comes from the upright angle and single inclined pylons are applicable to the diamond-shaped pylon. Therefore, it is necessary to conduct in-depth research for the diamond-shaped pylon, especially for lateral seismic fragility analysis [29].

In Section 1, an example cable-stayed bridge with diamond concrete pylon is introduced and the finite element model is developed by using the SAP2000 analysis platform. Section 2 introduces the component and system fragility analysis method used in this paper. Section 3 studied the limit states definition for the critical sections. The selected earthquake records from the PEER database for the IDA analysis are presented firstly. The critical sections for each component are determined by the value of the demand-capacity ratio. Finally, the limit states of each component are quantified. Section 4 presents the probabilistic estimation result of the bridge. Sections 5 and 6 introduce the component and system fragility analysis results of the example bridge subjected to the transverse excitations. The final section provides a brief summary with conclusions of the present study.

2. Case Study Cable-Stayed Bridge

2.1. Prototype Bridge. A typical cable-stayed bridge with diamond-shaped pylon is taken as the prototype bridge in this study, as illustrated in Figure 2(a). The case study bridge has a main span of 680 m and two side spans of 300 m. The streamlined steel box girder, with a width of 30.1 m and a depth of 3.5 m, is shown in Figure 2(b). The steel box girder is made of steel with a yield stress of 370 MPa. The girder is supported by 168 stayed cables with a fan-type cable arrangement and 16 steel spherical bearings (Figure 2(c)). Each cable is constituted by 109 galvanized steel wires whose diameter is 7 mm. The elasticity modulus of the stayed cables is 1.95×10^5 MPa and its standard strength is 1670 MPa. The steel spherical bearings are designed to connect the girder and pylons (or piers). The key dimensions of bearings are as follows: $A = 790$ mm, $D = 640$ mm, $E = 680$ mm, and $C = 830$ mm, as shown in Figure 2(c). The vertical bearing capacity of the steel spherical bearings is designed as 9000 kN. The deck can move freely in the longitudinal direction, but it is restrained in the transverse direction by wind-resistance bearings. The height of the RC diamond-shaped pylon is 220 m, and two pylon legs are connected by three crossbeams at the height of 48.6 m, 146.6 m, and 220 m. The diamond-shaped pylons are divided into three parts by the three crossbeams, that is, lower legs, middle legs, and upper legs. The heights of the three legs are 48.6 m, 98 m, and 67.4 m, and corresponding inclined angles are 100 degrees, 85 degrees, and 85 degrees, respectively. The inclined legs consist of hollow thin-walled box sections with variable dimensions. Six critical sections of the inclined legs for diamond-shaped pylons are shown in Figure 2(d) in detail. The pylons are made of C50 concrete with an elastic modulus of 3.45×10^4 MPa and compressive strength of 22.4 MPa.

2.2. Numerical Model. A three-dimensional FE model of the prototype cable-stayed bridge is established in SAP2000N platform. Figure 3 schematically shows the FE model of the prototype cable-stayed bridge. In the FEM model, the frame elements are adopted to represent pylons and piers. The torsional moment of the pylons is from 1191.6 m^4 to 195.3 m^4 in lower legs, from 185.7 m^4 to 168.6 m^4 in middle legs, and from 167.2 m^4 to 95.9 m^4 in upper legs. The inertial moments of the pylons around the y-axis are from 1181.7 m^4 to 704.3 m^4 in lower legs, from 691.0 m^4 to 241.8 m^4 in middle legs, and from 238.2 m^4 to 164.4 m^4 in upper legs. The inertial moments of the pylons around the z-axis are from 691.7 m^4 to 116.9 m^4 in lower legs, from 110.4 m^4 to 73.5 m^4 in middle legs, and from 73.2 m^4 to 68.4 m^4 in upper legs. The frame elements are used to represent the girder. The torsional moment of the girder is 7.45 m^4. The inertial moments of the girder around the y-axis and z-axis are 119.3 m^4 and 2.75 m^4, respectively.

All cables and girder are connected by the rigid link. Rigid link is modeled as an ideal rigid element with infinite stiffness. The elasticity modulus and inertia moment of the rigid element are usually set to be much large values than cables and girder. To be specific, the elasticity modulus of the rigid link in this FE model is 2.1×10^9 MPa, and its inertia moment around the y-axis and the z-axis are 1000 m^4 and 1000 m^4, respectively. The spherical steel bearing is represented by the Plastic-Wen constitutive model for simulating the deck-pylon connection which can be calculated as $f = r \cdot k \cdot d + (1 - r)\sigma_y \cdot z$, where k is the elastic spring stiffness; σ_y is yield stress; r is the ratio of postyield stiffness to elastic stiffness; z is an internal lag variable, $|z| \leq 1$ and $|z| = 1$ represent the yield surface. In this model, the yield force of elements is equal to critical sliding friction which can be calculated as $F_y = W \cdot u_d$. In the equation, W is the bearing weight of the support; u_d is the coefficient of sliding friction, which is set to be 0.2 in this paper.

The masses of the deck are lumped at the nodes of the girder with taking into account the mass moment of inertia. With respect to the cables, they are simulated by cable element and set the strength limitation considering the tension-only property. Furthermore, initial strain is applied to the element to take into account the initial stress of the stay cables.

The influence of the adjacent girder is considered by applying a vertical force of 1.11×10^6 N at the top nodes of pier #0 and pier #7, which is equal to half weight of the adjacent girder. The pylons and the piers are fixed at the bottom and the effect of soil-pile interaction is ignored. All degrees of freedom of the nodes at the bottom of the pylons and piers are set as fixed to simulate the fixed boundary of the prototype bridge. There are a total of 1879 nodes and 2043 elements in the whole FE model.

For the elastoplastic FE model, the plastic hinge element is used to simulate the elastoplastic damage process of the pylons or piers. Since only bending failures are allowed in the pylons/piers design, the M-M plastic hinges are set to the critical section of pylons/piers to analyze the elastoplastic state of the prototype bridge when suffered from severe earthquakes. The position, parameters, and number of plastic hinges set by the model will be introduced in Section 3.2.

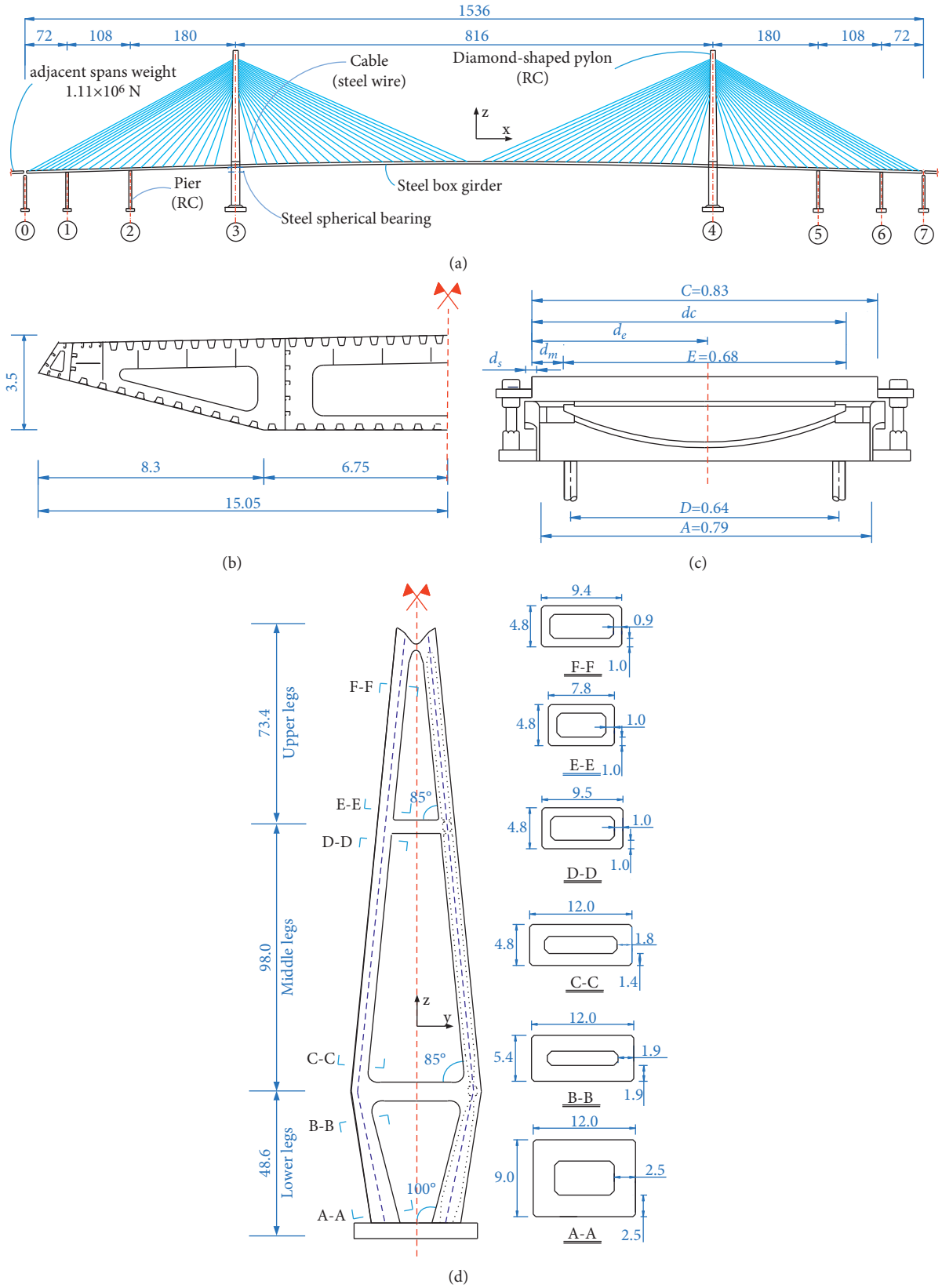

FIGURE 2: Overview of prototype bridge (unit: m). (a) General view of the cable-stayed bridge. (b) Cross section of the steel box girder. (c) Steel spherical bearing (QZ9000SX). (d) Diamond-shaped pylon.

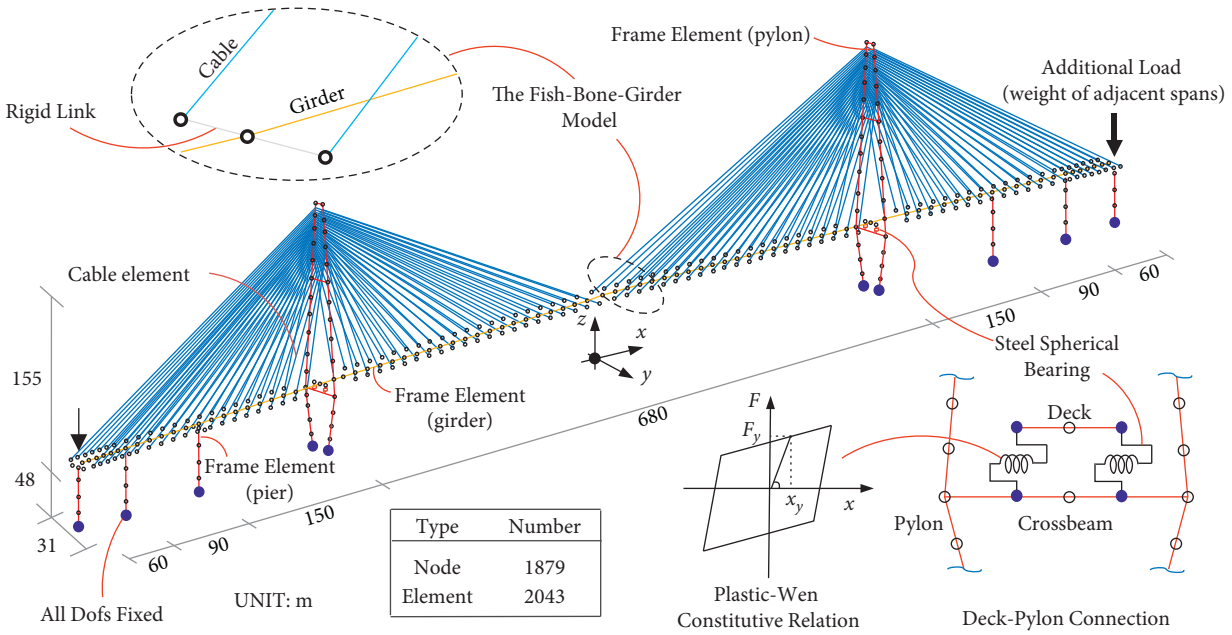

Figure 3: Finite element model of cable-stayed bridge.

3. Fragility Methodology

3.1. Component Fragility Function. The seismic fragility function is considered as the conditional failure probability of reaching or exceeding a specified damage state of an engineering structure for a given ground motion intensity. To develop fragility functions, the relationship between peak seismic responses and ground motion intensities (IMs) is required. Currently, there are two most common methods, the cloud approach and the scaling approach, to develop fragility functions based on nonlinear dynamic analysis [30]. For the sake of convenience, this paper used the scaling approach to develop the component fragility functions in this paper.

Based on the scaling approach, the vulnerability probability P_f of structures can be calculated as follows [9]:

$$\begin{aligned} P_f &= P\left[D \geq C_i \mid \mathrm{IM}\right] = 1 - P_f\left[D < C_i \mid \mathrm{IM}\right] \\ &= 1 - \int_{-\infty}^{C_i} u(D) f(D) \mathrm{d}D, \end{aligned} \tag{1}$$

where D is the maximum seismic demand and C_i is the ith critical damage level. The maximum seismic demand D can be calculated as

$$\begin{aligned} D &= a \cdot \mathrm{IM}^b \\ \text{or} \ln D &= b \ln \mathrm{IM} + \ln a, \end{aligned} \tag{2}$$

in which $\ln a$ and b are two coefficients obtained by the least squares linear regression of the ground motion intensity (IM) and the seismic demand D [31].

For the convenience of expression, the seismic demand (D) is usually expressed in logarithmic form. Based on [32], the equation can be express as follows:

$$P_f = P\left[\ln D \geq \ln C_i \mid \mathrm{IM}\right] = \Phi\left[\frac{\ln \mathrm{IM} - \ln \mu_{\mathrm{IM}}}{\sigma}\right], \tag{3}$$

$$\sigma = \sqrt{\sigma_{D|\mathrm{IM}}^2 + \sigma_C^2}, \tag{4}$$

where μ_{IM} is the median value of ground motion intensity (IM), corresponding to 50% damage probability. $\sigma_{D|\mathrm{IM}}$ and σ_C are the logarithmic standard deviations of the seismic demand of the structure (D) and the seismic capacity of the structure (C), respectively. According to this method, the probabilistic seismic demand model is built by combining the earthquake demand parameters with corresponding intensity parameters [33].

3.2. Bridge System Fragility Function. It has been proven that the bridge system is more vulnerable than any individual component [34]. Therefore, the component fragilities cannot accurately characterize the fragility of the bridge system. It is necessary to take into account the contributions of multiple components to develop the system fragility.

n practical engineering, the bridge structure can be conservatively assumed to be a serial system that consists of some interacting and interconnected components. Subsequently, the failure probability of a bridge system P_{sys} can be written as follows [35]:

$$\begin{aligned} P_{\mathrm{sys}} &= P\left(F_1 \cup F_2 \cup \cdots \cup F_m\right) = 1 - \Phi(\beta, \rho) \\ &= 1 - \int_{-\infty}^{\beta_1} \int_{-\infty}^{\beta_2} \cdots \int_{-\infty}^{\beta_m} \frac{1}{(2\pi)^{m/2} |\rho|^{1/2}} \\ &\times \exp\left(-\frac{1}{2} X^T \rho^{-1} X\right) \mathrm{d}x_1 \mathrm{d}x_2 \cdots \mathrm{d}x_m, \end{aligned} \tag{5}$$

where $F_i\,(i = 1, 2, 3, \ldots, m)$ = individual failure event; m is the number of failure components; $\Phi(\beta, \rho)$ is an m-dimensional multivariate normal cumulative distribution function; $\beta = (\beta_1, \beta_2, \ldots, \beta_m)$ is the vector of the reliability index of multiple components; $X(x_1, x_2, \ldots, x_m)$ is the m-dimensional vector of the normalized random variable x_i; and $\rho = \rho_{ij}\,[m \times m]$ is the correlation matrix of different failure components. It should be noted that the computation of $\Phi(\beta, \rho)$ is a critical step for determining. It can be calculated by a direct numerical integration method, a boundary estimation method, or an approximation method. It is worth mentioning that the calculation method is usually the same as the component fragility analysis in Section 2.1.

3.3. Seismic Fragility Analysis Procedure. Based on different data sources, seismic fragility curves are divided into three major types [9]: empirical fragility curves, expert-based fragility curves, and analytical fragility curves. Since the computational effort of the probabilistic seismic demand analysis method is less than the frequency statistics analysis method, the probabilistic seismic demand models based on the incremental dynamic analysis (IDA) method are adopted to develop the analytical fragility curves of the case study cable-stayed bridge in this study. The analysis procedures of this method are as follows:

(1) *Step 1*. Build the numerical model of the target bridge. Study the transverse seismic performance of pylons and piers by the capacity demand ratio method. Determine the vulnerable sections of pylons and piers to represent the seismic performance of components.

(2) *Step 2*. Select adequate ground motion records according to the site conditions of the case study bridge. Then scale the selected ground motions to 15 levels with PGA changes from 0.1 g to 1.5 g with 0.1 g increment.

(3) *Step 3*. Determine damage indexes of the components corresponding to different damage states.

(4) *Step 4*. Conduct nonlinear time-history analyses for the bridge structure subjected to the above ground motions with different intensity.

(5) *Step 5*. Based on the probabilistic seismic demand model proposed by Cornell et al. [36], the seismic demand D is combined with corresponding ground motion parameters PGA. The relationship is given in equation (2), in which a and b are regression coefficients determined by the least square method for fitting the time-history response data.

(6) *Step 6*. The probability density functions of the seismic demand parameter D and capacity parameter C of the bridge structure are assumed to follow log-normal distributions, the exceeding probability of structural damage is calculated by equation (3).

(7) *Step 7*. Develop firstly the fragility curves for the multiple components, and then they were combined into the system fragility curves which represent the seismic performance of the entire cable-stayed bridge through the first-order boundary method.

4. Limit States Definition for the Critical Sections

4.1. Input Ground Motions. The prototype bridge is located on the site of class III. Two seismic levels, level I earthquake (P1, $T_r = 1{,}000$ years) and level II earthquake (P2, $T_r = 2{,}500$ years), have been considered in the design of the prototype bridge. According to the site conditions, the peak ground accelerations (PGA) for level I and level II were 0.10 g and 0.22 g, respectively, which was developed by the Earthquake Engineering Research Institute of Fujian Province. Site-specific response spectra (assuming 5% damping) for level II earthquakes were shown in Figure 4.

Due to the discrete nature of earthquakes, a great number of ground motions were needed to achieve a better seismic fragility analysis result. The above response spectra for level II are employed as the target spectrum for matching suitable earthquake ground motions from the Pacific Earthquake Engineering Research Center (PEER) Strong Motion Database. As a result, 10 strong motions with magnitudes of 6.0–7.5 were selected. All of them come from the site of class III with equivalent shear wave velocity which is in the range of 109–192 m/s. Table 1 lists the selected earthquake records. Figure 4 shows the comparison between acceleration response spectra of the selected earthquake records (red dashed line) and the target response spectrum (black thick line).

4.2. Determine Critical Sections. It will result in high computation time and massive data if every pylons and piers section were taken into account in the vulnerability analysis. Therefore, it is necessary to find out a small number of critical sections for vulnerability analysis. The demand to capacity ratio method is recommended by Federal Highway Administration (FHWA) [37] to evaluate the seismic performance of bridges. This method evaluates the seismic performance of bridges by seismic demand to capacity ratio (D/C) of key structural components. The capacity demand ratio of the pylon and piers takes is expressed by

$$R_M = \frac{M_y}{M_{dd} + M_{td}}, \tag{6}$$

where R_M is the demand to capacity ratio (D/C) of the pylon or pier; M_y is the initial yield bending moment of the pylon or pier; M_{dd} is the dead load bending moment of the component; M_{td} is the maximum seismic bending moment of the component. When R_M is less than 1.0, the structure can be judged in the elastoplastic state.

Clearly, the seismic capacity is the key parameter in the demand to capacity ratio method. Existing studies have shown that most of the failure modes of pylons and pylons are bending failures [38]. The bending moment-curvature relationship is greatly affected by the axial force of the section. Therefore, the axial force of the critical section that suffered the earthquake excitation is studied. For example,

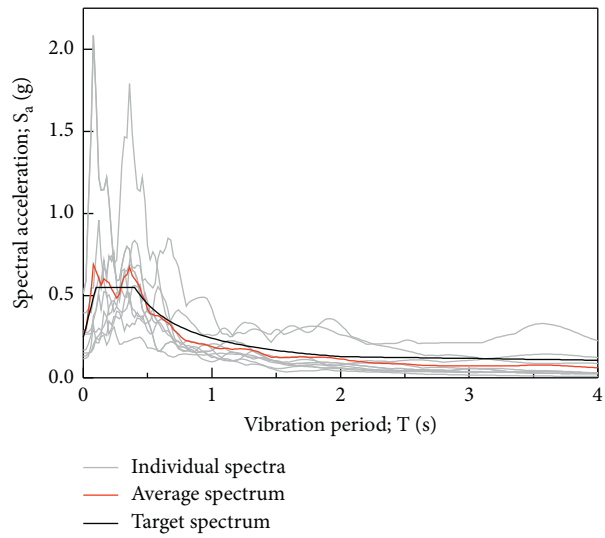

Figure 4: Acceleration response spectrum for selected records.

Table 1: Selected ground motion records from PEER database.

No.	Magnitude	Year	Earthquake event	Station	Motions component	PGA (g)
1	6.53	1979	Imperial Valley-06	Cerro Prieto	IMPVALL.H_H-CPE147	0.168
2	6.93	1989	Loma Prieta	Coyote Lake Dam	LOMAP_CYC195	0.152
3	7.01	1992	Cape Mendocino	Fortuna-Fortuna Blvd	CAPEMEND_FOR000	0.117
4	7.28	1992	Landers	Joshua Tree	LANDERS_JOS000	0.274
5	6.69	1994	Northridge-01	Sunland-Mt Gleason	NORTHR_GLE170	0.133
6	7.01	1992	Cape Mendocino	Loleta Fire Station	CAPEMEND_LFS270	0.265
7	7.37	1990	Manjil_Iran	Abbar	MANJIL_ABBARL	0.515
8	6.8	2007	Chuetsu-oki_Japan	Joetsu Ogataku	CHUETSU_65011NS	0.322
9	6.8	2007	Chuetsu-oki_Japan	NIG019	CHUETSU_NIG019NS	0.396
10	6.9	2008	Iwate_Japan	Tamati Ono	IWATE_54009NS	0.285

the axial force range of section T1 is shown in Figure 5. Because the axial force of the bridge tower under the dead load is very huge, the dynamic axial force excited by the level II earthquake is only within 6% of the dead load. It shows that the axial force of pylon induced by the earthquake is tiny compared to that of the dead load. Therefore, the axial force under dead load is used in bending moment-curvature capability analysis for convenience. Finally, the bending moment-curvature curve of the equivalent bilinear relationship and initial yield moment M_c was obtained.

The safety performance evaluation was carried out for the capacity demand ratio of the pylons and piers under earthquake excitations for level II. Firstly, the PGA of all ground motion was modulated to level II. Secondly, seismic response analysis was carried out for the cable-stayed bridge model and the envelope value of the bending moment along the height of the pylons and piers was obtained. Then, the average value of the bending moment envelope of the pylons and piers sections was calculated. Finally, applying the maximum seismic bending moments and the dead load bending moments, the capacity demand ratio R_m curve of each section along the height of the pylons and piers can be developed from equation (6), as shown in Figure 6.

As shown in Figures 6(a) and 6(b), under the earthquake of level II, the minimum capacity demand ratios of pylons and piers are greater than 1.0, indicating that pylons and piers are in the elastic state. As for the diamond-shaped bridge pylon, it can be observed from Figure 6(a) that peak

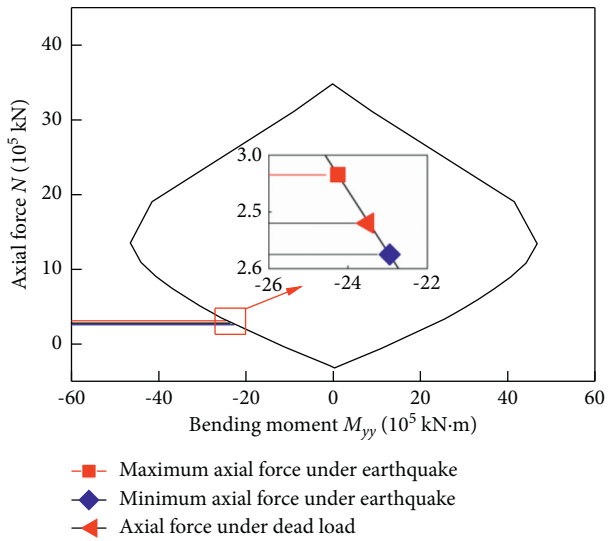

Figure 5: Moment capacity of section T1 corresponding to different axial force.

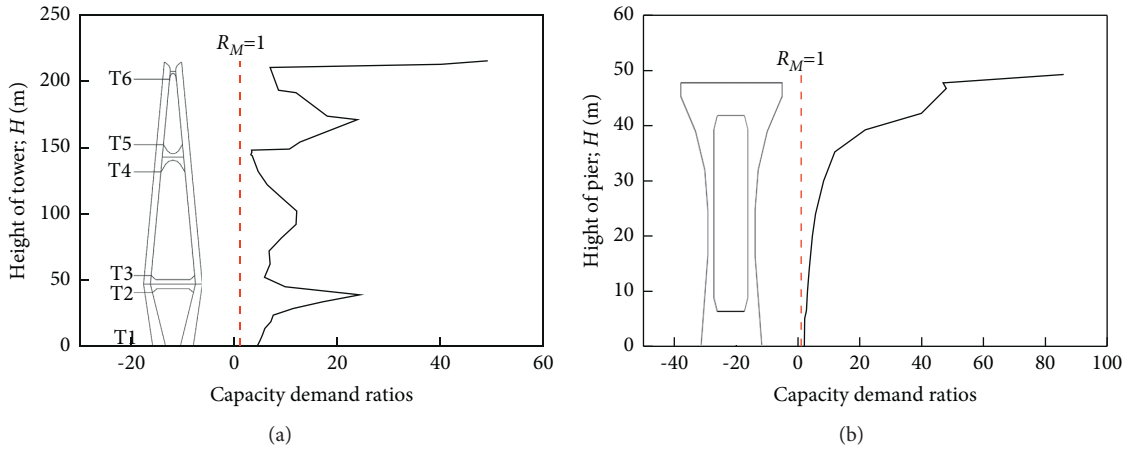

Figure 6: Demand-capacity ratios (D/C) curves for different components. (a) Pylon. (b) Pier #0.

values happen on sections around pylon bottom (section T1), near lower crossbeam (sections T2 and T3), near middle crossbeam (sections T4 and T5), and upper crossbeam (section T6). Comparing with the other regions, the capacity demand ratios of these four positions are closer to the critical boundary $R_M = 1$, which indicates that these four regions are the vulnerable parts. Moreover, among the four vulnerable regions, the capacity demand ratio of the bottom section of the middle transverse beam is closest to the critical value 1. Therefore, the bottom section of the middle transverse beam was selected as the vulnerable section to represent the seismic performance of the pylons. As for the bridge pier, however, the capacity demand ratio increases continuously along the height of the pier, as shown in Figure 6(b). It is obvious that the bottom section of the pier is the most vulnerable part. Therefore, the bottom section of the pier is selected to represent the seismic performance of the bridge pier.

The fragile sections of pylons and piers are simulated with the plastic hinge model. Figure 7 shows the distributions of plastic hinges in the SAP2000 model. Figure 8 illustrates the moment-curvature relationship of plastic hinges. In the figure, the key points B, C, D, and E represent yield point, peak value point, residual capacity point, and ultimate point, respectively. In the equation, φ_y represents initial yield curvature; φ_u represents ultimate yield curvature; M_y represents initial yield moment; and M_u represents ultimate yield moment. According to the recommendation by the specifications for Seismic Design of Highway Bridges, the length of the plastic hinge l_p can be calculated by the equation

$$l_p = \min\left\{0.08l + 0.022d_s f_y, \frac{2}{3}h\right\}, \tag{7}$$

where d_s and f_y are diameter and yield strength of the longitudinal reinforcing bars; l is the height of pier; and h is the height of the section. In the equation, the minimum value was selected as the length of the plastic hinge l_p in the seismic design.

The parameters of plastic hinges for critical sections in pylons and piers are listed in Table 2.

4.3. Define Limit States and Damage Index. The cable-stayed bridge contains pylon, pier, bearings, girder, and stay cables. The girder and the stay cables are expected to remain in the elastic even subjected to a strong earthquake. Previous shake table test [39] and numerical simulation [40] also show the pylons, piers, and bearings are critical responses for the cable-stayed bridge subjected to typical near-fault and one far-field ground motions. Thus, the fragility analysis was carried out only for the pylons, piers, and bearings in this paper.

The section curvature φ was adopted as the damage index for the pylons and piers in this paper. The states of the pylons and piers are defined into four different limit states (LSs) as follows: slight damage (SD), moderate damage (MD), extensive damage (ED), and complete damage (CD). The damage indicator of each LS was calculated through moment-curvature analyses for each critical section by XTRACT software. The damage indicator for each LS is shown in detail. For the slight damage state, the indicator is defined as the curvature of the reinforcing bar when first yielding (ϕ_{y1}). For the moderate damage state, the indicator is defined as the curvature of the section when plastic hinges appear in structural components (φ_y). For the extensive damage state, the indicator is defined as the curvature corresponding to concrete strain $\varepsilon_c = 0.004$ after the structural strength starts to decline (φ_{c4}). For the critical curvature threshold of the complete damage state, the indicator is defined as the curvature of the ultimate curvature. The relationship of the section moment and curvature in different damage states is shown in Figure 9.

The bearing is the most vulnerable component of the bridge structure. Usually, relative deformations are adopted as the fragility indexes of the bearings in other fragility studies. In this study, the transverse deformations between pylon and beam are adopted as the damage index of the bearings. The designed allowable deformations d_s of bearing are defined as the critical value of bearing under slight damage. The distance d_m between the ending of the upper plate and the ending of the spherical cap liner plate is defined as the critical value of moderate damage. The distance d_e between the ending of the upper plate and the centerline of the spherical cap liner plate is

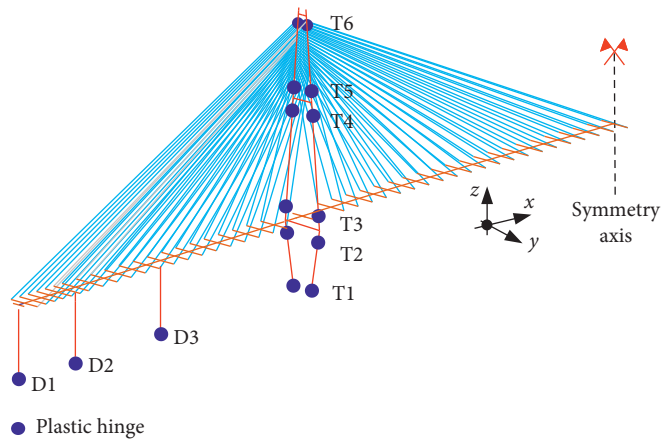

Figure 7: Distribution of plastic hinges.

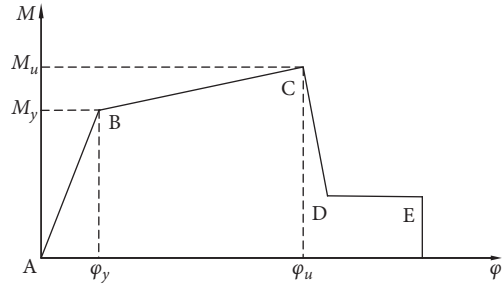

Figure 8: Moment-curvature curve for plastic hinges.

Table 2: The parameters of plastic hinges for critical sections.

Component	Plastic hinge	N (1/m)	φ_y (1/m)	φ_u (1/m)	M_y (kN·m)	M_u (kN·m)	l_p (m)
Pylons	T1	$2.76E+05$	$2.63E-04$	$1.53E-02$	$1.83E+06$	$2.76E+06$	6
	T2	$2.20E+05$	$4.61E-05$	$2.13E-02$	$8.44E+05$	$1.23E+06$	3.663
	T3	$1.93E+05$	$5.37E-04$	$2.38E-02$	$6.70E+05$	$9.84E+05$	3.221
	T4	$1.22E+05$	$4.91E-04$	$2.90E-02$	$4.01E+05$	$5.61E+05$	3.211
	T5	$1.15E+05$	$5.03E-04$	$2.91E-02$	$3.86E+05$	$5.41E+05$	3.221
	T6	$1.05E+04$	$4.29E-04$	$2.75E-02$	$2.23E+05$	$3.62E+05$	3.211
Piers	D1	$4.32E+04$	$2.51E-04$	$1.50E-02$	$3.16E+05$	$5.28E+05$	6
	D2	$3.53E+04$	$2.49E-04$	$1.49E-02$	$3.53E+05$	$5.67E+05$	6
	D3	$3.67E+04$	$2.49E-04$	$1.49E-02$	$3.58E+05$	$5.74E+05$	6

defined as the limit value of extensive damage. The distance d_c between the ending of the upper plate and the other ending of the spherical cap liner plate is defined as the critical value of complete damage. Four damage critical distances d_s, d_m, d_e, and d_c are shown in Figure 2(c).

According to the conclusions in Section 3.2, the vulnerable sections of pylons and piers are the bottom section of the middle transverse beam and the section of the pier bottom, respectively. Therefore, section T4 is employed to represent the seismic capacity of the bridge pylon. The seismic performance of pier #0, pier #1, and pier #2 is characterized by section D1, section D2, and section D3, respectively. By the above definition method of limit states, the quantified limit states of various components are listed in Table 3.

5. Probabilistic Estimation of Seismic Responses

In this paper, the PGA is utilized as the intensity measure (IM) for each record. The PGA of all ground motion records is scaled from 0.1 g to 1.5 g with an increment of 0.1 g. As a result, a total of 150 ground motions are obtained. In order to obtain the seismic demand of the structure under earthquake excitation, the probabilistic seismic demand analysis of the structure is carried out. First, transverse seismic demand analysis is performed using the dynamic increment method for the cable-stayed bridge model. The maximum seismic demand of each component is obtained corresponding to different PGA. And then, regression analysis is carried out in which the

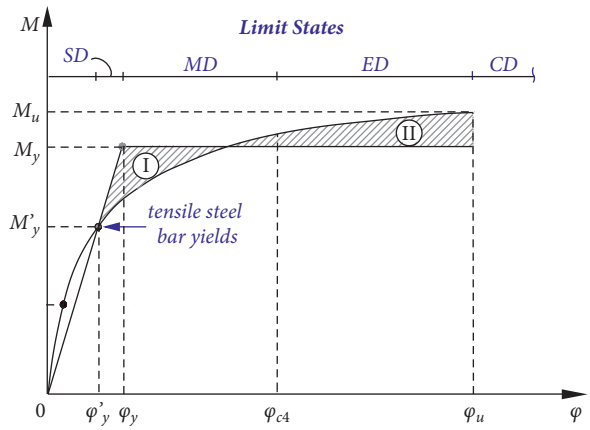

Figure 9: Critical curvatures of pylons and piers in each LS.

Table 3: Quantified damage index for different limit states.

Component	Damage index	Limit states			
		SD	MD	ED	CD
Pylon	Curvature (1/m)	0.49	0.65	10.60	29.00
Pier #0		0.25	0.33	5.05	15.00
Pier #1		0.25	0.33	5.18	14.90
Pier #2		0.25	0.33	5.19	14.90
Bearing	Deformation (mm)	20	75	415	755

Ln(PGA) and Ln(Φ), Ln(d) are taken as independent and dependent variables, respectively. Regression analyses of seismic demand for each component are shown in Figure 10.

6. Seismic Fragility Analysis of Components

According to equation (3), applying the formula obtained by probabilistic seismic demand models and the damage indexes of components under different damage states, the fragility curves under different seismic intensities can be developed, as shown in Figure 11.

As shown in Figures 11(a) and 11(b), under the slight and moderate damage, the order of the damage probability for all components is as follows: bearing (pier #0), bearing (pylon), pier #0, pier #1, pylon, and pier #2. When PGA is equal to 0.22 g, corresponding to the level II earthquake, the damage probabilities of pier #0, pylons, bearing (pier #0), and bearing (pylon) under slight damage are 34.5%, 8.89%, 67.6%, and 61.5%, respectively. However, under moderate damage, the corresponding damage probabilities decrease to 26.7%, 6.1%, 31.3%, and 21.2%, respectively. When PGA is equal to 0.7 g, the damage probabilities of bearing under slight damage and moderate damage are up to 99.6% and 96.8%. It indicates that the damage state of bearing is sensitive to PGA. Moreover, it can be observed from Figures 11(c) and 11(d) that the damage probability of the piers #0 is the highest in various components of the example bridge under the extensive and complete damage, followed by the pylons, pier #1, pier #2, and bearing (the pylons).

When subjected to a level II earthquake, the components of cable-stayed bridge rarely suffer from extensive and complete damage. Thus, failure probability equal to 50% was adopted as the exceeding damage probability to assess the fragility of different components. Taking the bottom of pier #0 as an example shown in Figures 11(c) and 11(d), the PGA for the 50% probability is 0.8 g for extensive damage state, while PGA increases to 1.2 g for the complete damage state. It indicates that the component has good ductility.

7. Seismic Fragility Analysis of Bridge System

The bridge structure is a complex structural system. Thus, it is necessary to simplify the bridge system into an ideal reliability model to investigate the fragility of the bridge system. The lower bound in this equation determined by the maximum component fragility represents the probability of failure for the entire system, while the upper bound is the combination of the component fragility. The lower and upper bounds of the fragility curves under different damage states calculated by the first-order boundary method [24] are shown in Figure 12.

Comparing the bridge system fragility in Figures 12(a) and 12(b), it can be observed that the fragility curves of bridge system on the lower bound and upper bound show little difference in SD states and MD states. However, for the ED state and CD state, the difference of the fragility curves on the lower bound and upper bound is apparent because the failure probability of each component is various in the latter two states.

It should be noted that the fragilities of the bearings are the closest to the system fragilities of the bridge, followed by the fragility of the piers and the fragility of the pylons. It

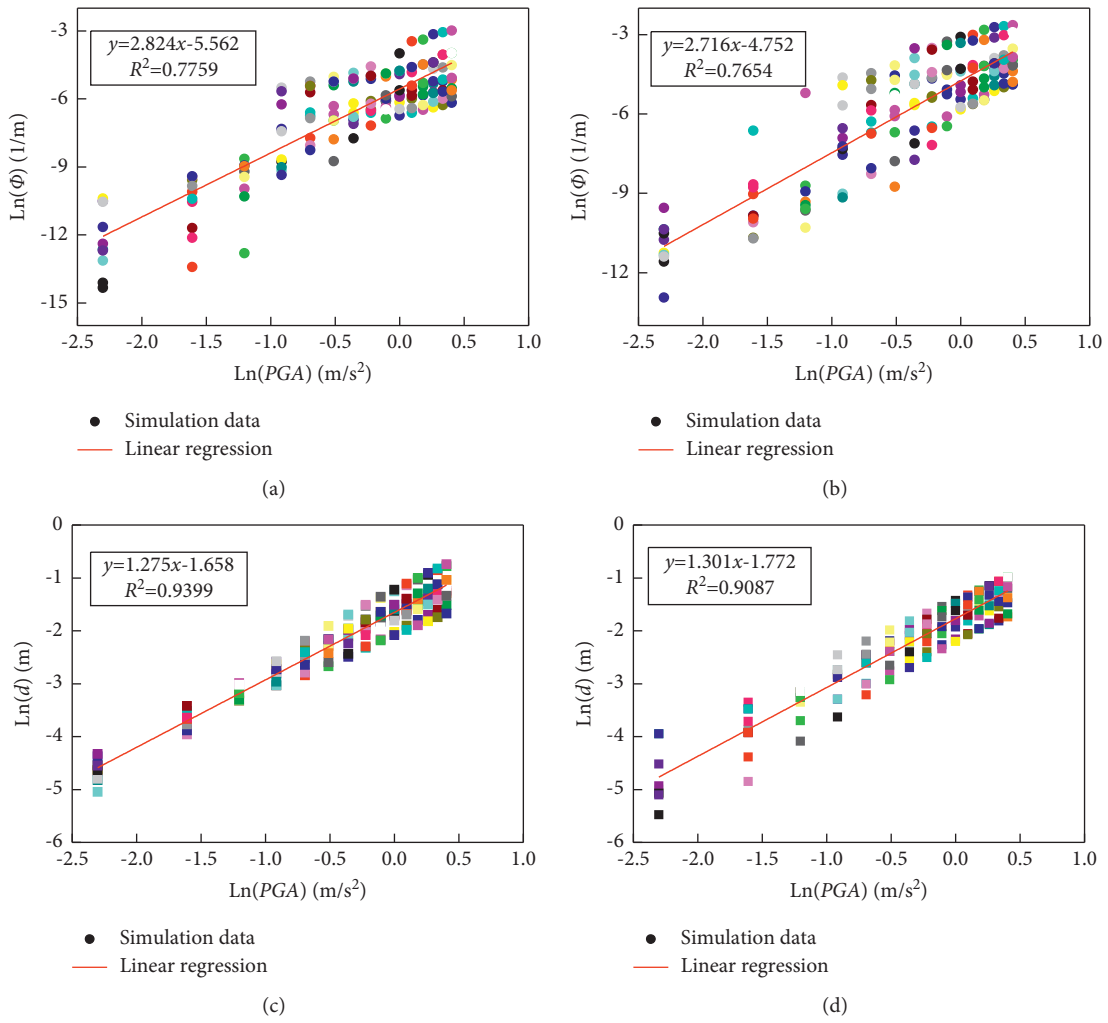

Figure 10: Regression analysis of seismic demand. (a) Curvature of sec. T4 in pylon. (b) Curvature of sec. D1 in pier. (c) Deformation between pylon and girder. (d) Deformation between pier #0 and girder.

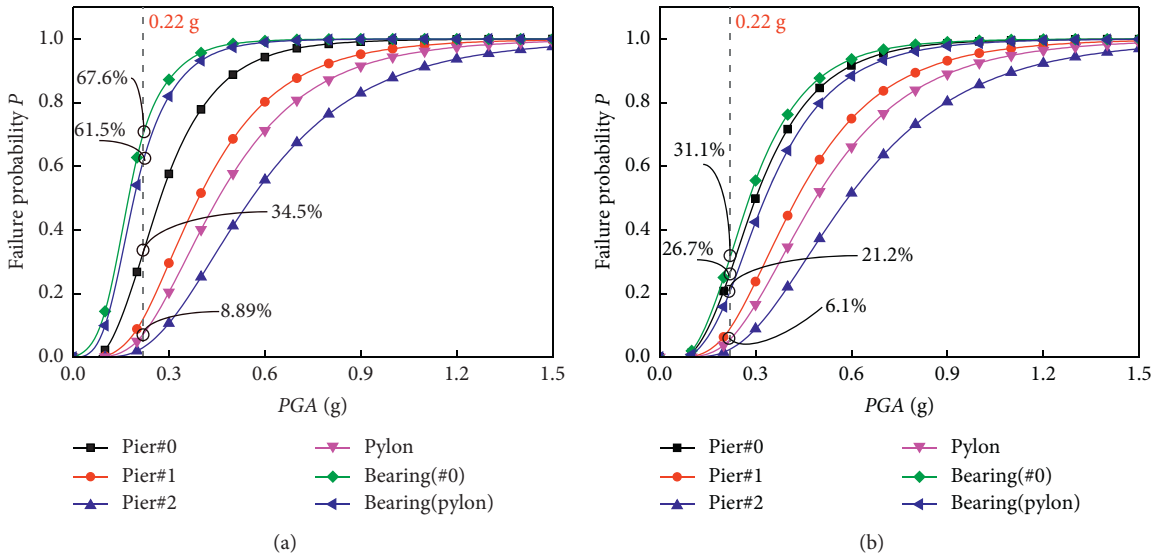

Figure 11: Continued.

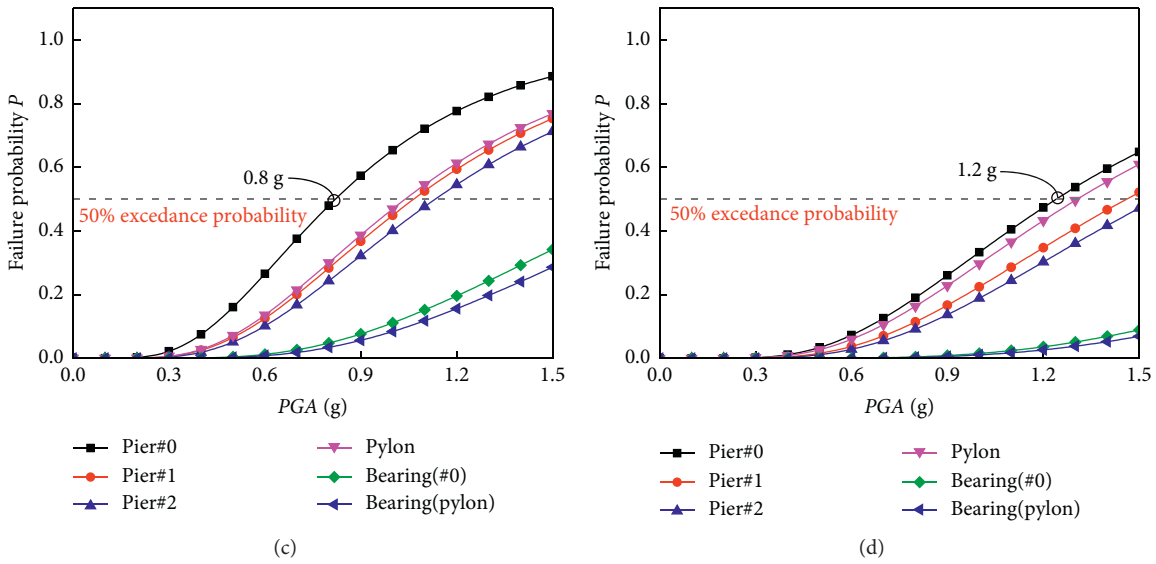

Figure 11: Component fragility curves in different limit states. (a) Slight damage. (b) Moderate damage. (c) Extensive damage. (d) Complete damage.

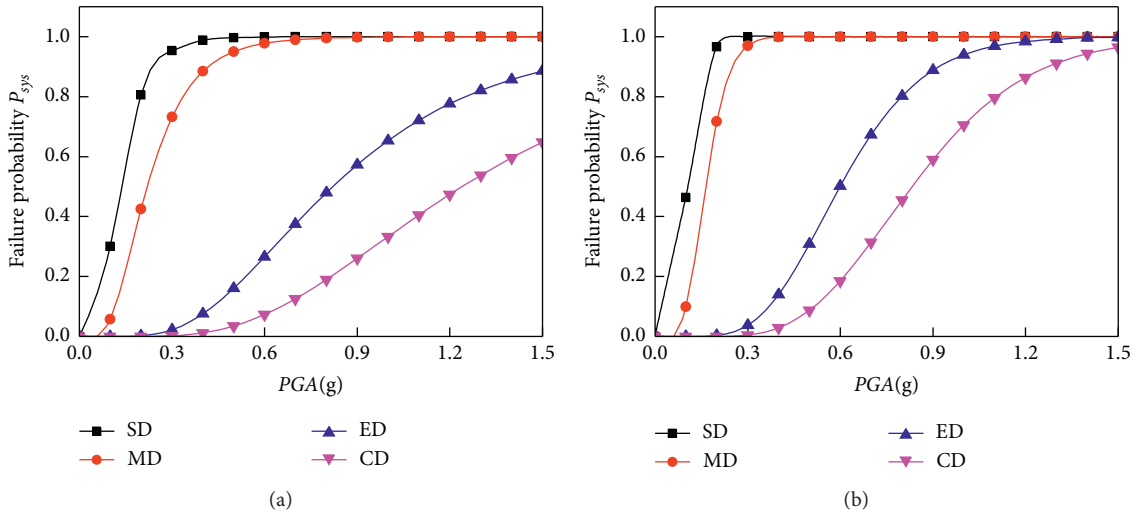

Figure 12: The bridge system fragility curves. (a) Lower bound. (b) Upper bound.

indicates that the proximity of the fragility curves of components to the system fragility curves is inversely proportional to the importance of components.

It can be concluded that the entire cable-stayed bridge is prone to suffer from slight damage and moderate damage. Moreover, the system fragility of the entire bridge is larger than the fragility of any individual component in the system. Therefore, it will bring errors to the bridge system fragility assessment using component fragilities to represent the entire bridge.

8. Conclusions

This study presents the lateral seismic fragility assessment of cable-stayed bridge with diamond concrete pylons. A typical cable-stayed bridge with a diamond-shaped pylon is taken as the prototype bridge. A three-dimensional FE model of the prototype CSB is established in SAP2000N platform. Based on the capacity demand ratios, the vulnerable sections of pylon and piers are indicated. All vulnerable sections are simulated by the plastic hinge in the FEM according to the bending moment-curvatures. For the CSB, four different limit states (LSs) and damage index are defined for each component. Through the probabilistic estimation and seismic fragility, the following conclusions can be drawn from this study:

(1) Based on capacity demand ratio analysis, the lateral vulnerable sections of the diamond-shaped pylon are identified as sections near the middle crossbeam (sections T4 and T5), around the pylon bottom (sections T1), and near the lower crossbeam (sections T2 and T3).

(2) Seismic fragility analysis of each component shows that the order of the damage probability is bearing (pier #0), bearing (pylon), pier #0, pier #1, pylon, and pier #2 in the slight damage (SD) and moderate damage (MD) states. The damage probability of bearing is sensitive to PGA. The damage probability of the piers #0 is the highest, followed by the pylons, pier #1, pier #2, and bearing (the pylons) in the ED and CD states,

(3) Seismic fragility analysis of bridge system shows that the fragility curves of bridge system on lower bound and upper bound show little difference in SD states and MD states. However, those are apparent in ED and CD states as the failure probability of each component is various in the latter two states. The entire cable-stayed bridge is prone to suffer from slight damage and moderate damage. Moreover, the system fragility of the entire bridge is larger than the fragility of any individual component in the system.

Data Availability

No data were used to support this study.

Disclosure

The results and conclusions presented in the paper are those of the authors and do not necessarily reflect the view of the sponsors.

Conflicts of Interest

The author declares that there are no conflicts of interest regarding the publication of this paper.

Acknowledgments

The authors would like to acknowledge the funding from the National Natural Science Foundation of China (no. E51508102), the Natural Science Foundation of Fujian Province (Grant no. 2019J01233), and the Fuzhou University Testing Fund of Precious Apparatus (Grant 2020T035).

References

[1] C. Zhang, J. B. Lu, H. Y. Jia, Z. C. Lai, L. Xu, and P. G. Wang, "Influence of near-fault ground motions on seismic response of long-span cable-stayed bridge," *Bulletin of Earthquake Engineering*, vol. 18, no. 14, 2020.

[2] C. Zhang, G. Fu, Z. Lai et al., "Shake table test of long span cable-stayed bridge subjected to near-fault ground motions considering velocity pulse effect and non-uniform excitation," *Applied Sciences*, vol. 10, no. 19, Article ID 6969, 2020.

[3] C. Zhang and K. Huang, "Influence law of tower stiffness on vertical stiffness of three-tower self-anchored suspension bridge based on frequency formulas," *Journal of vibroengineering*, vol. 16, no. 6, pp. 2908–2919, 2014.

[4] Y. Xu, X. Duan, and J. Li, "Seismic design strategy of cable stayed bridges subjected to strong ground motions," *Structural Engineering & Mechanics*, vol. 51, no. 6, pp. 51–73, 2014.

[5] Q. Han, J. Wen, X. Du, Z. Zhong, and H. Hao, "Simplified seismic resistant design of base isolated single pylon cable-stayed bridge," *Bulletin of Earthquake Engineering*, vol. 16, no. 10, pp. 5041–5059, 2018.

[6] J. Yi and J. Li, "Experimental and numerical study on seismic response of inclined tower legs of cable-stayed bridges during earthquakes," *Engineering Structures*, vol. 183, pp. 180–194, 2019.

[7] S. S. Patil and J. P. Patankar, "Seismic response of cable stayed bridge with different types of pylons of various heights," *International Journal of Advanced Research and Development*, vol. 4, no. 2, 2017.

[8] M. D. Martínez-Rodrigo and A. Filiatrault, "A case study on the application of passive control and seismic isolation techniques to cable-stayed bridges: a comparative investigation through non-linear dynamic analyses," *Engineering Structures*, vol. 99, pp. 232–252, 2015.

[9] C. Zhang, C. W. Wu, and P. G. Wang, "Seismic fragility analysis of bridge group pile foundations considering fluid-pile-soil interaction," *Shock and Vibration*, vol. 2020, Article ID 8838813, 17 pages, 2020.

[10] K. C. Chang, Y. L. Mo, C. C. Chen, L. C. Lai, and C. C. Chou, "Lessons learned from the damaged Chi-Lu cable-stayed bridge," *Journal of Bridge Engineering*, vol. 9, no. 4, pp. 343–352, 2004.

[11] T. Takeda, T. Mizutani, T. Nagayama, and Y. Fujino, "Reproduction of cable-stayed bridge seismic responses involving tower-girder pounding and damage process estimation for large earthquakes," *Journal of Bridge Engineering*, vol. 24, no. 2, Article ID 4018112, 2019.

[12] L. Xu, K. Liu, C. Zhang, J. H. Zheng, C. Wang, and Q. Huang, "Experimental study of seismic mitigation of large-span cable-stayed bridges with elastic cables by shaking table test," *Practice Periodical on Structural Design and Construction*, vol. 26, 2020.

[13] D. Zhang, N. Li, S. Zhang, and Z.-X. Li, "Energy dissipation and resilience of precast segmented concrete-filled steel tube self-centering column: parameter study and design methodology," *Engineering Structures*, vol. 244, Article ID 112747, 2021.

[14] H.-Y. Jia, X.-L. Lan, S.-X. Zheng, L.-P. Li, and C.-Q. Liu, "Assessment on required separation length between adjacent bridge segments to avoid pounding," *Soil Dynamics and Earthquake Engineering*, vol. 120, pp. 398–407, 2019.

[15] L. Xu, H. Zhang, J. Gao, and C. Zhang, "Longitudinal seismic responses of a cable-stayed bridge based on shaking table tests of a half-bridge scale model," *Advances in Structural Engineering*, vol. 22, no. 1, pp. 81–93, 2018.

[16] E. N. Tochaei, T. Taylor, and F. Ansari, "Effects of near-field ground motions and soil-structure interaction on dynamic response of a cable-stayed bridge," *Soil Dynamics and Earthquake Engineering*, vol. 133, Article ID 106115, 2020.

[17] W. Xie and L. Sun, "Transverse seismic response and failure mode of towers of a cable-stayed bridge full-model: tests and simulations," *Engineering Failure Analysis*, vol. 122, Article ID 105224, 2021.

[18] Q. Han, J. Wen, X. Du, and C. Huang, "Seismic response of single pylon cable-stayed bridge under scour effect," *Journal of Bridge Engineering*, vol. 24, no. 6, Article ID 5019007, 2019.

[19] X. Wang, J. Fang, L. Zhou, and A. Ye, "Transverse seismic failure mechanism and ductility of reinforced concrete pylon for long span cable-stayed bridges: model test and numerical analysis," *Engineering Structures*, vol. 189, pp. 206–221, 2019.

[20] Y. Xu, R. Wang, and J. Li, "Experimental verification of a cable-stayed bridge model using passive energy dissipation devices," *Journal of Bridge Engineering*, vol. 21, no. 12, pp. 401–425, 2016.

[21] R. Wang, Y. Xu, and J. Li, "Transverse seismic behavior studies of a medium span cable-stayed bridge model with two concrete towers," *Journal of Earthquake Engineering*, vol. 21, no. 1, pp. 151–168, 2017.

[22] A. Camara and E. Efthymiou, "Deck-tower interaction in the transverse seismic response of cable-stayed bridges and optimum configurations," *Engineering Structures*, vol. 124, pp. 494–506, 2016.

[23] C. Zhang, G. H. Fu, Z. Ling, and C. Lin, "Influence of the tower shapes on lateral seismic response of cable-stayed bridge," *Earthquake Engineering and Engineering Dynamics*, vol. 40, no. 3, pp. 97–110, 2020.

[24] W. Wu, L. Li, and X. Shao, "Seismic assessment of medium-span concrete cable-stayed bridges using the component and system fragility functions," *Journal of Bridge Engineering*, vol. 21, no. 6, Article ID 4016027, 2016.

[25] H.-Y. Jia, W.-Q. Yue, S.-X. Zheng, H.-Y. Gou, C.-H. Zhao, and G. You, "Time-dependent pounding probability analysis between adjacent decks of bridges under non-stationary stochastic seismic excitations," *Structure*, vol. 28, pp. 2355–2366, 2020.

[26] K. Porter, R. Kennedy, and R. Bachman, "Creating fragility functions for performance-based earthquake engineering," *Earthquake Spectra*, vol. 23, no. 2, pp. 471–489, 2007.

[27] C. Li, H.-N. Li, H. Hao, K. Bi, and B. Chen, "Seismic fragility analyses of sea-crossing cable-stayed bridges subjected to multi-support ground motions on offshore sites," *Engineering Structures*, vol. 165, pp. 441–456, 2018.

[28] J. Zhong, J.-S. Jeon, and W.-X. Ren, "Risk assessment for a long-span cable-stayed bridge subjected to multiple support excitations," *Engineering Structures*, vol. 176, pp. 220–230, 2018.

[29] C. Li, H. Hao, H. Li, and K. Bi, "Seismic fragility analysis of reinforced concrete bridges with chloride induced corrosion subjected to spatially varying ground motions," *International Journal of Structural Stability and Dynamics*, vol. 16, 2015.

[30] Z. Jian and Y. Huo, "Evaluating effectiveness and optimum design of isolation devices for highway bridges using the fragility function method," *Engineering Structures*, vol. 31, no. 8, pp. 1648–1660, 2009.

[31] E. Choi, R. Desroches, and B. Nielson, "Seismic fragility of typical bridges in moderate seismic zones," *Engineering Structures*, vol. 26, no. 2, pp. 187–199, 2004.

[32] A. Martínez, M. A. Hube, and K. M. Rollins, "Analytical fragility curves for non-skewed highway bridges in Chile," *Engineering Structures*, vol. 141, pp. 530–542, 2017.

[33] C. J. F. H. Cornell, "Probabilistic basis for 2000 sac federal emergency management agency steel moment frame guidelines," *Journal of Structural Engineering*, vol. 4, no. 526, pp. 526–533, 2002.

[34] B. G. Nielson, *Analytical Fragility Curves for Highway Bridges in Moderate Seismic Zones*, Ph.D. thesis, Georgia Institute of Technology, Atlanta, Georgia, 2005.

[35] X.-X. Yuan and M. D. Pandey, "Analysis of approximations for multinormal integration in system reliability computation," *Structural Safety*, vol. 28, no. 4, pp. 361–377, 2006.

[36] C. A. Cornell, F. Jalayer, R. O. Hamburger, and D. A. Foutch, "Probabilistic basis for 2000 SAC federal emergency management agency steel moment frame guidelines," *Journal of Structural Engineering*, vol. 128, no. 4, pp. 526–533, 2002.

[37] I. G. Buckle and I. M. Friedland, "A seismic retrofitting manual for highway bridges," *Center for Earthquake Engineering Research (NCEER)*, pp. 249–258, National Center for Earthquake Engineering Research (NCEER), Buffalo, NY, US, 1994.

[38] A. Camara, R. Cristantielli, M. A. Astiz, and C. Málaga-Chuquitaype, "Design of hysteretic dampers with optimal ductility for the transverse seismic control of cable-stayed bridges," *Earthquake Engineering & Structural Dynamics*, vol. 46, no. 11, pp. 1811–1833, 2017.

[39] L. Zhou, X. Wang, and A. Ye, "Shake table test on transverse steel damper seismic system for long span cable-stayed bridges," *Engineering Structures*, vol. 179, pp. 106–119, 2019.

[40] F. Liang, Y. Jia, W. Xie, L. Sun, and H. Chen, "Transverse response of pile group foundations supporting a long-span cable-stayed bridge under uniform and nonuniform excitation," *Soil Dynamics and Earthquake Engineering*, vol. 121, pp. 57–74, 2019.